Journal of Metals, Materials and Minerals, Vol.28 No.2 pp.1-10, 2018

Consideration of key process parameters for achieving robust and uniform cutting of Ti-6Al-4V sheet metal using fiber laser with nitrogen assisted gas

Varit POSHYANANDA[1,*], Jidsucha DARAYEN[1], Krittima TUMKHANON[1], Chedtha PUNCREOBUTR[1,2], Atchara KHAMKONGKAEO[1], and Boonrat LOHWONGWATANA[1,2,**]

[1]*Advanced Material Analysis Research Unit, Department of Metallurgical Engineering, Faculty of Engineering, Chulalongkorn University, Bangkok, Thailand*
[2]*Biomedical Engineering Program, Biomedical Engineering Research Center, Faculty of Engineering, Chulalongkorn University, Bangkok, Thailand*

***Corresponding author e-mail:** *avarit.po@student.chula.ac.th and **bboonrat.l@chula.ac.th

Received date:
10 April 2018
Revised date:
3 July 2018
Accepted date:
3 August 2018

Keywords:
Titanium
Ti-6Al-4V
Laser Cutting
Recast Layer
Heat-Affected Zone

Abstract

In laser cutting, to work on sensitive and intricate materials, such as titanium, requires rigorous control of parameters to achieve the best cutting results due to high power throughput and rapid cutting speed. Titanium is known for severe reaction with oxygen and nitrogen at elevated temperatures, however the more inert argon assist gas is cost prohibitive in commercial application. To achieve cut quality using nitrogen as an assist gas in titanium cutting, careful control is needed to prevent the formation of hard and brittle martensite as well as nitride- and oxide- phases. To better understand the roles of industrial grade raw materials and assist gas in commercial laser cutting, phase transformation, heat affected zone (HAZ) cut quality and the relationships amongst parameters have been selected to mimic industrial setups. 2mm thick titanium sheet was cut by a fiber laser cutting process using nitrogen assist gas by varying three cutting parameters including (i) laser power (1000-3000 watts), (ii) cutting speed (4000-26000 mm/min), and (iii) assist gas pressure (1-20 bars). Cut quality assessment was interpreted through the scanning electron microscope (SEM) and optical observation to link with mechanical properties from bending and v-notch fracture tests. The results showed that increase in cutting speed will limit the thickness of heat-affected zone (HAZ) which varied from 20-500 um. Pressure of the assist gas should be above a threshold value of 8 bar to assure complete ejection of the liquid melt pool. Key observations were reported along with root causes, such as, (i) non-uniformed and thick HAZ layer, (ii) thick and brittle recast (RC) layer, as well as (iii) micro-tearing due to localized expansion of nitrogen rich phase.

1. Introduction

Ti-6Al-4V alloy is an engineering titanium alloy widely used in the aerospace and biomedical industries due to its high strength to weight ratio, excellent corrosion resistance, formability and biocompatibility. There are several manufacturing processes for titanium alloys such as machining, casting, additive manufacturing and laser cutting. In particular, laser cutting could produce intricate 2D parts with high productivity. Laser cutting is considered to be a non-contact process, yet, there are potential complications due to titanium's reactions with surrounding gases as well as induced phase transformation.

In order to achieve reliable cutting quality, cut kerf and surrounding surfaces should be investigated in depth. Physical phenomena such as laser power absorption, heating and cooling effects, reactions of titanium with gaseous species, viscosity rise of the melt pool due to temperature increase, etc., are important and requiring in-depth analysis of the final microstructures.

Heat-affected zone (HAZ) refers to the area where temperature arises over phase transformation or recrystallization temperature. Possibly inequilibrium fast cooling would result in phase transformation and the production of new microstructure. Recast layer (RC) is a layer of material that solidifies from liquid-phase. In particular for titanium, the formation of HAZ and RC will be more complex because of titanium's high affinity to nitrogen and oxygen at temperatures over 200°C [1]. Nitrogen is generally used as assist gas during cutting to repel

DOI: 10.14456/jmmm.2018.19

molten liquid. Argon gas could replace nitrogen to achieve nitride-free cut surface, but argon consumption could make the cutting process cost prohibitive. Furthermore, in many factories the machine has already installed with oxygen and nitrogen assisted gas supply system. Nitrogen can use as an assist gas for titanium cutting but some reaction can occur. Additionally, previous studies suggested that nitrogen assist gas could create more uniform HAZ layer with smoother cut surface in the case of titanium sheet cutting [2]. The assist gas repels molten metal out of cut region, then heat dissipates by conduction to lower temperature base metal. The remaining liquid must also solidify in a fraction of second. If the temperature of a region near the melt pool raised above beta-transus temperature (995°C for Ti-6Al-4V) [3] titanium could change its atomic structure from alpha-phase (HCP: Hexagonal-close packed) to beta-phase (BCC: Body-centered cubic). High cooling rate might trigger the non-equilibrium martensitic phase transformation which is typically hard and brittle. Within the liquid phase, while nitrogen assist gas assures abundant supply of nitrogen, titanium is highly reactive with nitrogen to form Nitride (TiN) layer. The formation leads to high residual stress at the surface [4] with microcrack formation as a result of fast cooling rate and differential thermal contraction due to nitride precipitation in RC layer [5-7]. At high temperature above 1200°C, TiN can also react with oxygen and transform to TiO_2 following the reaction: $2TiN + 2O_2 \rightarrow 2TiO_2 + N_2$ [8,9]. Both oxygen and nitrogen can diffuse into solid titanium at high temperatures [4] and stabilized the alpha phase. This special layer is called an alpha-case layer, which is hard and brittle [10,11]. When compared to oxygen, nitrogen has lower diffusion rate in titanium and the subsequent post-finishing processes had been proven less difficult in the case of nitrogen assist gas.

For laser cutting process parameters, three main variables with strong effects on the cut quality and cutting cost are (i) laser power, (ii) cutting speed, and (iii) assist gas pressure. Previous study on laser powers revealed the relationship between lower cutting quality and lower power laser. This was because the viscosity increases in the liquid melt pool which could be related to the lower laser power density and lower temperature. Higher viscosity liquid was more difficult to repel from cut areas [12]. Because of high cooling rate, laser cutting generally produced a cut region with high level of residual-stress [13,14]. When cutting speed increased, HAZ depth and residual-stress under a cut surface will decrease significantly [15-18]. Increased assist gas pressure did not directly relate to the increase in oxide formation. Rather the increase of excessive heat played a major role especially when the cutting head leaves the cutting region [19]. When all effects are combined, the investigation and analysis became challenging as the interactions amongst these phenomena are more difficult to separate.

Finally, the mechanical properties could be directly related to the crystal structures and microstructures. Four dominant phases are typically found in laser cut process of Ti-6Al-4V utilizing high laser power and rapid cooling. The microstructure of as-received Ti-6Al-4V sheet is binary in nature comprising of both alpha and beta phases.

The α phase, HCP structure, has high strength and toughness with no ductile to brittle transformation temperature. This phase is stable at temperature below 910°C for commercially pure Titanium. In the case of Ti-6Al-4V, the transformation temperature was raised to 995°C.
The β phase, BCC structure, has high toughness and ductility but lower strength. The phase is normally stable at above beta transus temperature. The BCC phase could be further stabilized by adding some alloying element such as vanadium, chromium and molybdenum.

The α′ phase, acicular martensitic structure, could be formed by a military decomposition of β phase. This metastable phase is hard and brittle in nature. The transformation takes place during rapid cooling of metal from above beta-transus temperature down to room temperature.

Finally, for the laser cutting, several technologies have emerged as laser sources that are suitable for different applications from engraving to guiding laser, and from cutting to additive manufacturing. In our case, Bystronic BySprint Fiber 3015 CNC cutting machine with ByFiber 3000 3kW fiber laser source is the workhorse for all experiments. Fiber laser was chosen because of an advantage over CO_2 laser such as small spot size, high power density, high efficiency and low maintenance cost. However, the shorter wavelength (1080 nm) compared to 10600 nm of CO_2 laser, the high cut quality of fiber laser will only be possible for thin sheet cutting. In high precision manufacturing process, the pre-forming to near net shape using of laser cutting could significantly reduce tools wear and eliminate the high production cost of machining process.

2. Experimental Procedure

2.1. Preparation of testing specimen

Titanium sheet has been cut following the schematic of 50x6x2 mm drawing shown in the Figure 1 by Bystronic BySprint Fiber 3015 CNC cutting machine with ByFiber 3000 3kW Fiber laser source. Fixed parameters were the raw material, 2-mm thick Ti-6Al-4V sheet, nitrogen assist gas, 1.5 mm nozzle diameter at 2 mm nozzle distant, and 0.3 mm focal depth. The first experiment was to identify the cutting speed limit of the machine by varying two parameters: minimum laser power and cutting speed. When the cutting speed was set, minimum laser power that allowed for a complete cut was identified. As the cutting speed increased, the minimum laser power linearly increased as shown in Figure 2. For the case of 2-mm thick titanium alloy sheet with predefined cut schematic, the machine cutting speed limit was approximately 24,000 mm/min. The limitation was due to the machine limitation.

Assist gas pressure range was then adjusted according to the lowest pressure that can repel molten metal from cut kerf to ensure a complete cut. Ranges of selected parameters are tabulated in Table. 1. Successful cut specimens were then further investigated in three main areas: (i) bending test, (ii) v-notch and (iii) microstructural investigation. Bending test parts were subjected to bending by hydraulic press-brake machine (Amada HS-1303). Bending was performed in the direction perpendicular to the cut direction and V-notch portion was broken at the cut surface to perform approximated ductility assessment. Microstructure investigation portion was mounted using Epoxy resin (Struers Epofix). The microstructure specimens were cross-sectioned and polished using series of SiC abrasive papers. Finally, fine polishing was achieved by utilization of custom mixture of 10% H_2O_2 and 0.05 um colloidal silica suspension (Buehler MasterMet).

2.2. Characterization

Penetration depth, HAZ and RC were inspected and measured by 3 depth levels using polarized optical microscope (Huvitz HRM-300) and Panasis software. Deviations of measured thickness were in the range of ± 5% which was adequate for quantitative analysis of cutting parameters. Specimens were etched in Kroll's reagent for 6 seconds before the cross-sectional microstructure was polished using metallography technique. Direct observation was done using an optical microscope and scanning electron microscope (Field Emission Scanning Electron Microscope, FESEM: FEI Quanta FEG 450). Energy dispersive x-ray spectroscopy technique (OXFORD X-act) was used in conjunction with FESEM to investigate the chemical composition in the specimen. The focus was on the elemental mapping for the analysis of the HAZ and RC layer to understand the nature and origin of reacted surface microstructures. Following a bending test, specimens were also investigated for relationship between the microstructure and mechanical behaviors.

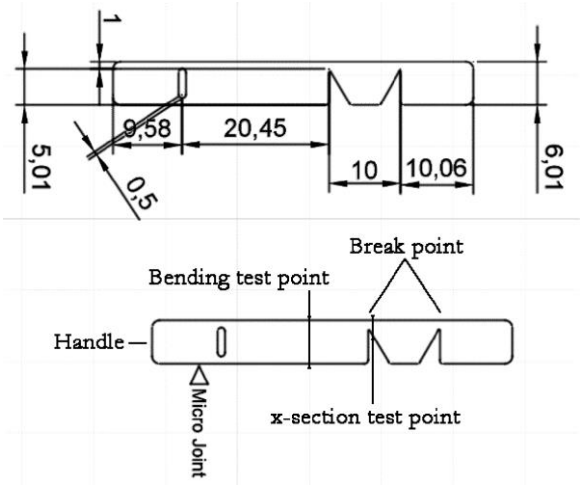

Figure 1. The schematic shows dimension and shape of designed workpiece in millimeters unit. Three main test specimens were created in one cutting experiment: (i) bending test, (ii) v-notch break and (iii) microstructural analysis.

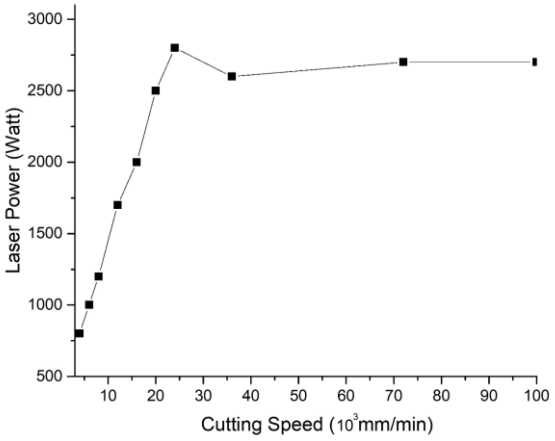

Figure 2. The graph plotted from experimental data to show the relationship between cutting speed and lowest laser power for successful cutting of 2 mm Ti-6Al-4V sheet using 16bar assist gas pressure. Actual cutting speed reached the limitation of machine acceleration at approximately 24,000 mm/min.

Table 1. Ranges of cutting parameters that were investigated in this experiment.

Parameters	
Assist gas pressure (bar)	1, 4, 6, 8, 12, 16, 20
Average output power (Watts)	1000, 1500, 2000, 2500, 3000
Speed (mm/min)	4000,6000, 8000, 12000, 16000, 20000, 24000
Nozzle orifice diameter (mm)	1.5
Nozzle to workpiece distance (mm)	2
Focus depth (mm)	0.3
Focus spot diameter (mm)	0.1
Laser wavelength (nm)	1080
Laser cutting mode	CW

3. Results and discussion

3.1 Laser parameters relationship

The development of a mathematical relationship for laser power required to cut a Ti-6Al-4V metal sheet can be explained by an energy conservation model as shown in Equation. 1 and plotted in Figure 3. Linear relationship between cutting speed (mm/min) and laser power (Watts) is plotted for the successful cutting of 2 mm-thick Ti-6Al-4V metal sheet.

The model expresses the correlation by assuming that energy required to raise the temperature of titanium cut volume to a melting point (and subsequently to melt in specific time) requires correction factor for power loss from chaotic phenomena, such as localized heat loss, spattering, superheating and vaporization etc. The required laser power could then be expressed as:

$P_{laser} = \frac{1}{k} P_{loss} \rho F w t (Cp(T_M - T_0) + L_m) + P_{m.loss}$, [Equation. 1]

when P_{laser} is the machine laser power required to cut successfully (Watts),

k is the wavelength absorption coefficient,
P_{loss} is the fractional power loss (unitless),
ρ is density (g/cm^3) of the metal,
F is the cutting speed *(*cm/sec),
w is the kerf width (cm),
t is sheet thickness (cm),
Cp is the heat capacity (J/g·K),
T_M is the melting point (K),
T_0 is the ambient material temperature (K),
L_m is the latent heat of melting (J/g) of Ti-6Al-4V, and finally
$P_{m.loss}$ is the power loss in machine system (Watts).

When substituted in the equation, the properties of Ti-6Al-4V are given as k = 0.4, ρ = 4.45 g/cm^3, w = 0.022 cm, t = 0.2 cm, Cp = 0.56 J/g·K, T_M = 1900 K, T_0 = 293 K and L_m = 365 J/g. The relation was found to be linear as shown in Figure 3 and the relationship can be fitted to the following equation:

P_{laser} (W) = 0.1032*Cutting Speed + 391, [Equation. 2]

when the unit of cutting speed is expressed in mm/min (according to the digital outputs shown on the machine for practicality).

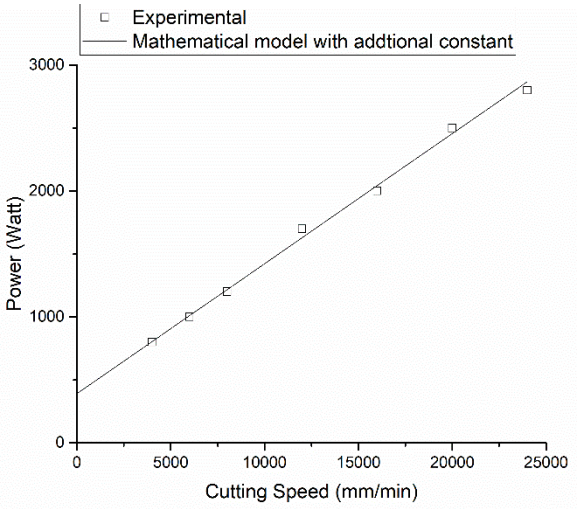

Figure 3. The experimental data was plotted with the mathematical model. Linear correlation between cutting speed (mm/min) and laser power (Watts) is plotted for the successful cutting of 2 mm thick Ti-6Al-4V metal sheet using 16 bar assist gas pressure.

3.2 Assist gas pressure

Assist gas plays an important role in a microstructural evolution and cut quality. Top and bottom regions of kerf cut were compared. When the assist gas pressure was below 6 bars, unequal penetration depths were found with non-uniform Heat-Affected Zone (HAZ). The side perpendicular to the cut surface was prepared for metallographic study and thickness measurements of HAZ and recast layer (RC) as shown in Figure 4. When the pressure was too low to propel the molten metal, thick RC layers were formed as a result. The residual heat in liquid was abundant and dissipation of heat to the base metal usually occur at the bottom of cut kerf and resulting in HAZ. If liquid was too hot, occasionally locally melt craters in the base metal was found. Laser cut kerf surfaces of 2 mm sheet Ti-6Al-4V were cut using various assist gas pressures. Left image, Figure 5, showed molten RC zone that could not be completely repelled from the cut at 1 bar assist gas pressure.

To further investigate the effects of assist gas pressure, HAZs in different regions of the kerf were found to have different thicknesses due to localized heating. The thicknesses were recorded in 3 regions: (i) top HAZ for the region towards the top surface where the laser first interacted with the material, (ii) middle HAZ for the middle region inside the sheet, and finally (iii) bottom HAZ for the region where liquid metal exited the kerf. The comparisons of three thickness regions when assist gas pressure ranged from 1 to 20 bars were compared in Figure 6.

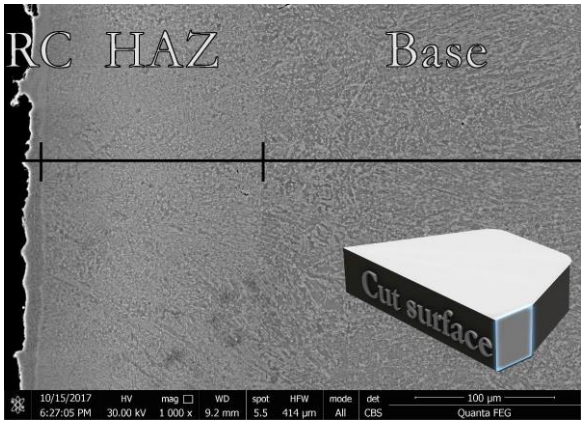

Figure 4. Cross-section of test specimen had been prepared for metallographic investigation using the following cutting parameters: 1,000 Watts power, 4,000 mm/min cutting speed and 8 bar assist gas. Three different regions are identified by their microstructures to be recast layer (RC), heat affected zone (HAZ) and base metal (Base). The inset shows the schematic of the area of investigation.

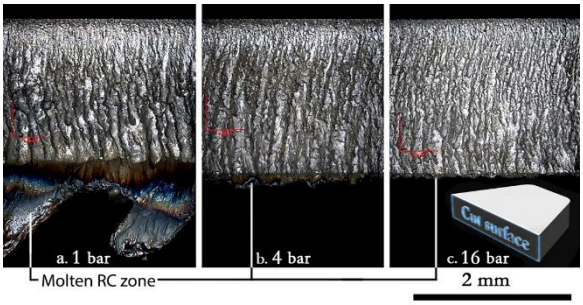

Figure 5. Laser cut kerf surfaces of 2 mm Ti-6Al-4V sheet were cut using various assist gas pressures. Left image showed molten RC zone that could not be completely repelled from the cut and caused deep penetration of HAZ. The sample was prepared by the following cutting parameters: 3,000 Watts power, 4,000 mm/min cutting speed and 8 bar assist gas.

Assist gas pressure strongly correlated to the thickness of the bottom HAZ. The difference in thickness of the top and bottom HAZ was also plotted as a function of assist gas pressure shown as the dotted line in Figure 6. Though the HAZ thickness difference became less prominent at high pressure, there was a double-sword effect. When the assist gas was higher than 20 bars, micro-tearing on a surface was observed due to turbulence and chaotic flow of the liquid metal and the assist gas. In our experiments, appropriate assist gas pressure was found to be in the range of 6 to 12 bars as it resulted in uniform HAZ thickness and acceptable cut quality with minute amount of N-rich phase in RC. Kerf size and laser spot size seemed to have direct relations with such turbulence effect, however these parameters were beyond the scope of this research.

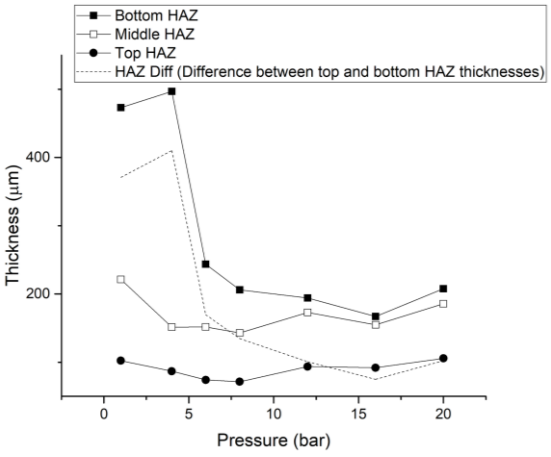

Figure 6. The graph shows the relationship between assist gas pressure (bar) and the thicknesses of HAZ from 3 different regions (top, middle and bottom) obtained from cutting experiment of 2 mm sheet of Ti-6Al-4V with 3,000W of laser power and 4,000 mm/min cutting speed. Dotted line shows the difference between top and bottom HAZ thicknesses.

3.3 Effect of cutting speed

The cutting speed was inversely proportional to the depth of HAZ. Careful observation revealed that, as the cutting speed increases, the molten metal in front of cutting kerf would be rejected quickly. Aside from shorter exposure time, the fast rejection of molten metal allowed for only shorter time for heat conduction. The HAZ layer was therefore shallower when compared to the case of lower cutting speeds. In one particular investigation, 8 and 16 bars assist gas pressure were utilized and the HAZ thicknesses were compared with different cutting speeds. There was a clear correlation of cutting speed and HAZ particularly when the assist gas pressure was at 8 bars. If the cutting speed could be maintained above 12,000 mm/min, both 8 and 16 bars assist gas produced good quality cut with similar HAZ thicknesses.

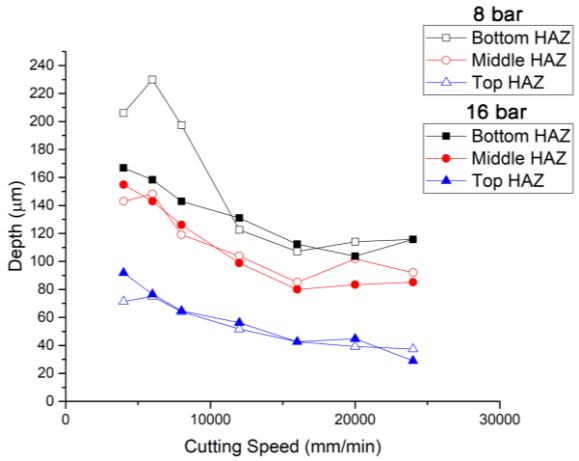

Figure 7. The relationship between cutting speed and HAZ depth is plotted from a cutting experiment utilizing 8 bars and 16 bars of assist gas pressure and 3,000 Watts laser power.

3.4 Effect of laser power

When laser power was below a threshold value, the resulting lower temperature of the melt pool could yield cutting defects due to incomplete liquid ejection. The melt pool liquid of lower temperature had higher viscosity, and during ejection, part of the liquid could layer themselves on top of one another on the kerf surface. Several cut kerfs revealed such evidence that the layers could not escape from the bottom of the kerf. As a result, the microstructure of nearby region showed significantly deeper and unequal HAZ. In the case of 2 mm thick titanium sheet cutting, when assist gas pressure above 12 bars was applied, the effect of laser power did not show strong correlation to the HAZ thickness. The sensitivity to laser power only revealed when the assist gas pressure was below 12 bars. For example, when assist gas was at 16 bars, the cut quality is immune to defects for all laser power ranging from 1000-3000 Watts as shown in Figure 8.

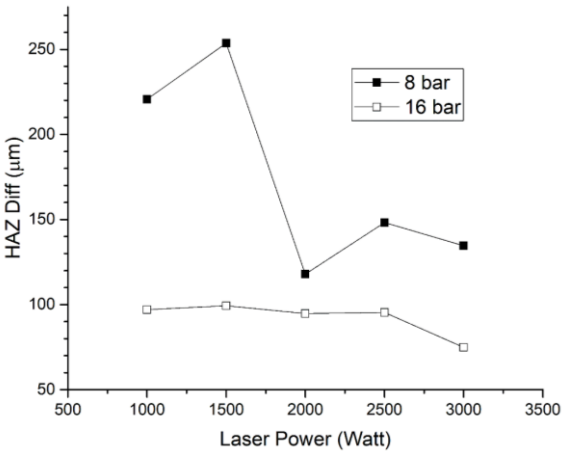

Figure 8. The difference in thickness between top and bottom HAZ is plotted as a function of laser power. Two assist gas pressures of 8 and 16 bars were compared for the cutting of 2-mm Ti-6Al-4V sheet. 4,000 mm/min cutting speed was used. The quality of cut, as expressed by difference in HAZ, was found to be poor and sensitive at 8 bars and below, and the effect is much less pronounced at 16 bars assist gas pressure.

3.5 Effects from oxygen and nitrogen

FESEM analysis revealed chemical compositions of the microstructure in the region around the cut. The kerf surface was found mostly to be thin nitride layer as shown as purple mapping in Figure 9b. with small amount of oxygen rich area. Thin nitride layer was formed during cutting when nitrogen was abundant. The left region in Figure 9b. represented the area near the top cut surface in which oxide compound was predominant (green area as shown in EDS mapping). In this near top surface region, titanium readily reacted with oxygen when assist nitrogen gas could no longer cover the fresh cut region. When cutting head left the region, titanium surface and RC layer were both exposed to the atmosphere while the metal continued to cool down from cutting temperature to below 600 K. Above 600 K, oxygen is known to react readily with titanium forming oxide layer of different stoichiometric compositions while nitrogen was depleted in this area. In particular, oxygen could dissolve and diffuse into titanium metal to form alpha case layer. The formation of layer could easily result in micro-cracks during cutting due to rapid volume change in localized constrained area. Ten to twenty micrometer thick RC layer with micro-cracks was revealed in SEM image in Figure 10a.

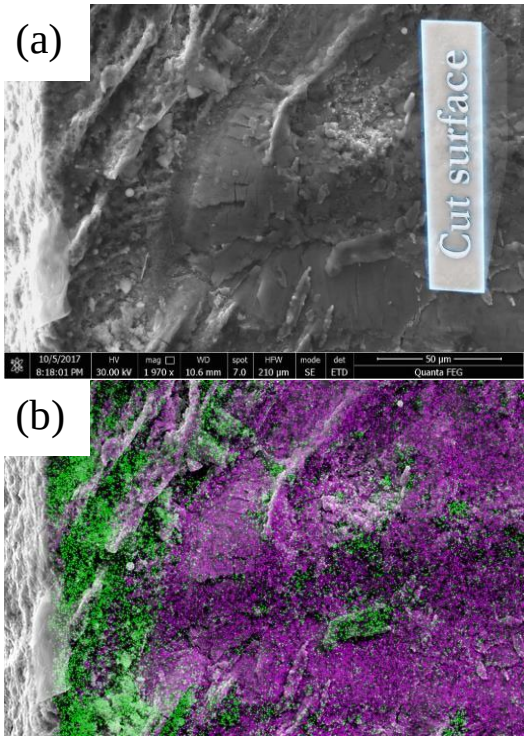

Figure 9. (a) SEM image shows the bottom surface of cut kerf and (b) EDS mapping of oxygen (green) and nitrogen (pink) distribution on surface (Cutting parameters: 3,000 Watts, 8 bars and 24,000 mm/min)

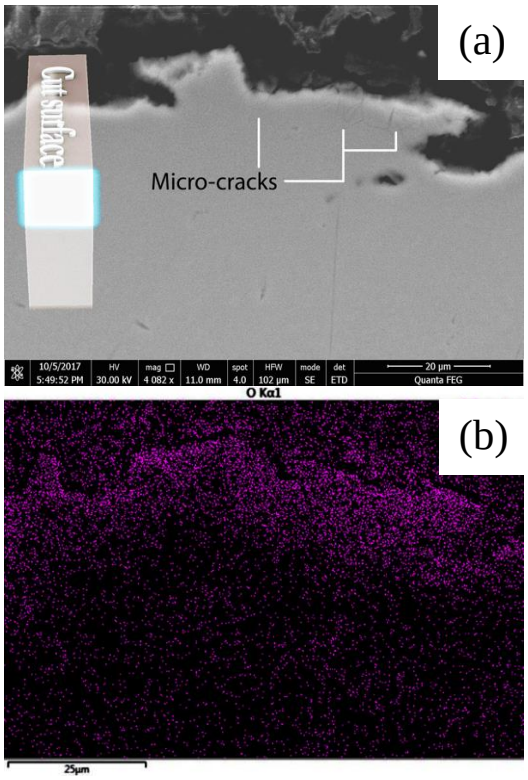

Figure 10. (a) SEM images revealed micro-cracks in a few regions at the surface of RC layer, and (b) The EDS mapping of the same region shows oxygen diffusion profile from the surface down. (Cutting parameters: 3,000 Watts, 8 bars and 24,000 mm/min)

Upon closer inspection of the surface area next and perpendicular to the cut surface, nitrogen-rich phases with nitrogen content at 10 At.% and above were found on the RC layer. Underneath the region covered by such nitrogen rich phases, martensite needles were abundant as shown in Figure 11a. The phase fraction of nitride-rich phase was related to the assist gas pressure, as shown in Figure 11a and Figure 11b, the increase in pressure from 1 bars to 16 bars would result in the increase in the amount of nitride rich phase.

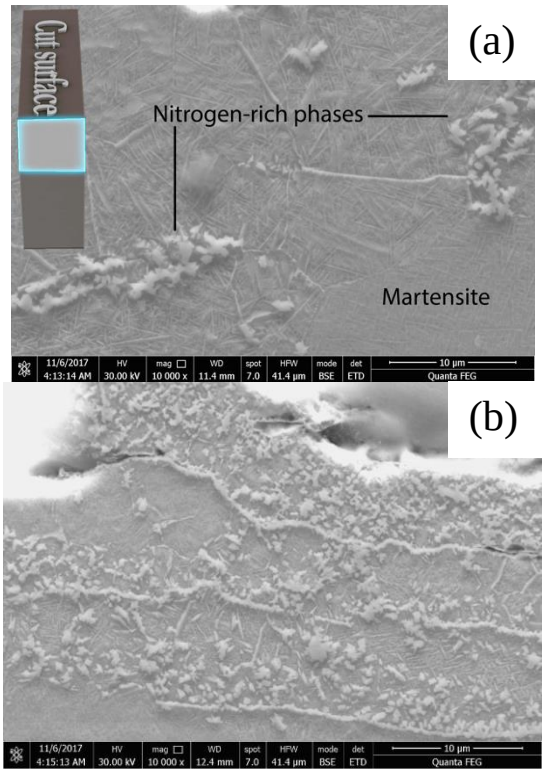

Figure 11. (a) SEM image reveals an RC layer with nitrogen-rich phases showing as light shade on the surface and a martensitic phase revealing on the background. The specimen was cut with 1 bar assist gas pressure. Small inset shows the schematic of the investigated face of the test specimen. (b) SEM image in a similar region which cut with 16 bars assist gas pressure showed higher percentage of nitrogen-rich phase. For both images, the cut surfaces are located at the top. The specimens were cut with the following parameters: 3,000 Watts laser power, 4000 mm/min cutting speed and 1 bar assist gas (top), and 3,000 Watts laser power, 4000 mm/min cutting speed and 16 bars assist gas (bottom).

An SEM inspection at lower magnification, shown in Figure 12., revealed 10-20 micron layered RC structure on the side perpendicular to the cut surface. Such layer structure was the result of shearing of liquid melt that deposited during the cutting. The investigation was done on these layers and nitrogen rich phase was found underneath newly melted layer.

These recast layers could be easily removed by polishing. The thickness of these layers was found to be correlated to the turbulence as a combined effect of assist gas pressure and cutting speed. For the HAZ, only martensite microstructure was found with no change in chemical composition as compared to as-received specimen.

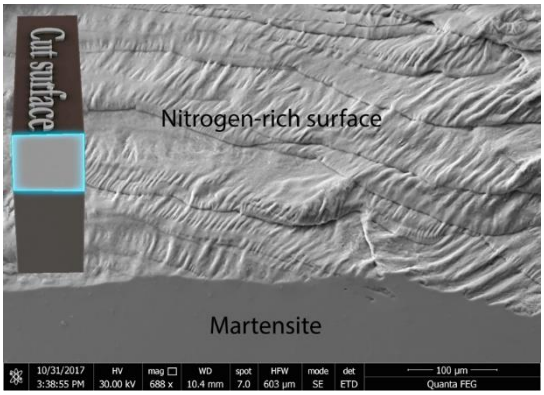

Figure 12. SEM micrograph reveals the layering structure of RC layer. The nitrogen rich region on the specimen surface was created by recasting, layer by layer. The specimen was prepared by the following parameters: 3,000 Watts laser power, 4,000 mm/min cutting speed and 8 bars assist gas pressure.

3.6 Bending and v-notch break tests

The schematic of bending specimen, as shown in Figure 13, was designed to accentuate the hardness and mechanical behaviors of various microstructures and cut surfaces. The microstructure as illustrated in Figure 13a and 13b was the qualitative evidence for brittleness of RC layer. Brittle RC layer was promptly separated from the HAZ layer underneath during bending as shown in Figure 13b. The root causes were believed to be the inclusion and volume expansion of nitride rich phase in the RC layer. In Figure 14, the specimens were subjected to a v-notch break test. SEM fractography revealed three different natures of surface morphology. Left most, RC layer was the most brittle amongst three, as the fracture was a clean cut. Severe separation could be found along the RC-HAZ interface as shown in the middle region of the fractography. Fracture nature in the HAZ region was predominantly clean and brittle in nature. To the right, dimple-type morphology was found as a typical indicator of ductile rupture for the base metal.

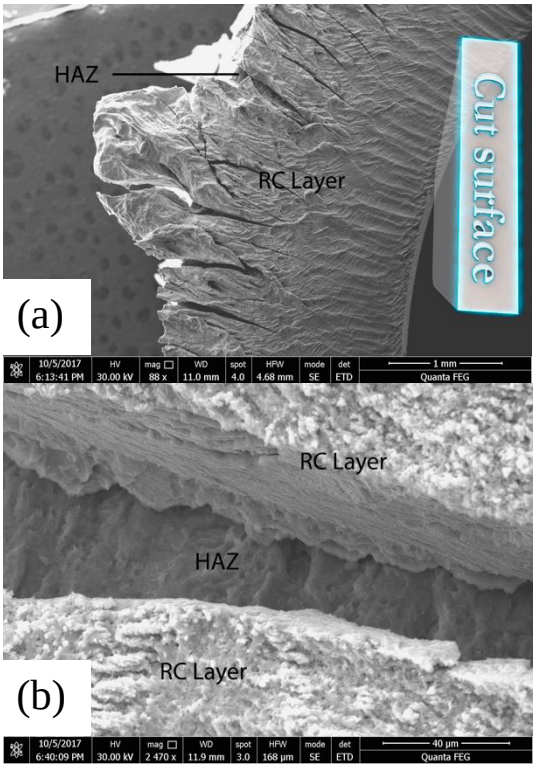

Figure 13. (a) RC layers were bent along the cut surface. The nitrogen-rich RC layer broke away easily and separated itself from the HAZ. Upon closer inspection in (b) HAZ region underneath did not break off (right). The inset shows the cut surface in which the SEM investigation was carried out. The specimen was prepared by the following parameters: 3,000 Watts laser power, 4,000 mm/min cutting speed and 8 bars assist gas pressure.

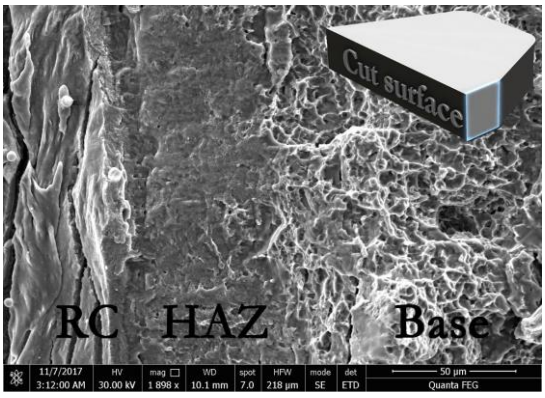

Figure 14. SEM image of the fracture revealed the fracture of RC, HAZ and base metal when specimen was broken by a qualitative v-notch test. The specimen was prepared by the following parameters: 3,000 Watts laser power, 4,000 mm/min cutting speed and 8 bars assist gas pressure.

4. Conclusions

Laser cutting is a fast and powerful manufacturing process. The amount of power being delivered to a cut is so large and abrupt that generated heat could be detrimental to the cut material. To optimize cutting parameters, the following conclusions have been developed based on traditional materials science tetrahedron framework linking performance, processing, microstructure and properties. The processing parameters, such as cooling rates, at cut surface. The martensitic phase transformation was evident in Ti-6Al-4V cut specimens leading to hard and brittle properties. Recast layer is the by-product of eject liquid melt that did not completely leave the cut. Our investigation revealed layered and alternating structure of rapidly cool Ti-alloy melt (martensitic) and separated nitrogen rich area. Additionally, there have been evidence of martensitic microstructure in the RC region confirming that the quenching rate of these RC layers is sufficient for martensitic transformation. In the area towards the top and bottom of the cut kerf, oxygen atoms diffuse into RC layers to approximately 15 microns depth. For the heat-affected zone, no chemical composition variation was detected. Aside from alpha and beta titanium, martensite was found in areas where quenching rate was higher than approximately 18°C s^{-1}.

For industrial applications, the parameters optimization in laser cutting process is a key to produce high accuracy and high-quality products. To enhance the quality of laser cutting, higher cutting speed is always good for production rate and shallow HAZ layer. However occasionally the geometry of the work piece and the machine capability were posed as a limit. Increasing the laser power will not increase the HAZ depth. However, the quality of the cut can be improved because higher temperature of molten metal has lower viscosity and therefore the liquid pool could be ejected out easily. Too high assist gas pressure leads to the increase in nitrogen-rich phase in RC layer. On the contrary, if the assist gas pressure is too low, HAZ and RC regions become large and irregular. The experiments showed that assist gas pressure at 8 bars is the best value for cutting 2 mm Ti-6Al-4V sheet. Finally, RC layer is physically more brittle than HAZ layer. Unlike the HAZ which can be eliminated by heat treatment and/or polishing, RC layer requires mechanical processes to remove.

5. Acknowledgments

The authors would like to thank Biomedical Engineering Research Center, and Advanced Material Analysis Research Unit, Faculty of Engineering, Chulalongkorn University, Thailand for providing SEM and EDS facilities. Atchara Khamkongkaeo would like to thank Rachadapisek Sompote Fund, Chulalongkorn University for her Postdoctoral Fellowship. This work is financially supported by Thai TGK Industry Corporation Limited, Thailand.

References

[1] D. P. Shidid, M. H. Gollo, M. Brandt, and M. Mahdavian, "Study of effect of process parameters on titanium sheet metal bending using Nd: YAG laser," *Optics & Laser Technology*, vol. 47, pp. 242-247, 2013.

[2] N. Andersson and C. Granberg, "Laser cutting in Ti-6Al-4V sheet: DOE and evaluation of process parameters Informative," Master Degree Thesis, Department of Materials and Manufacturing Technology, Chalmers University of Technology: Gothenburg, Sweden, 2015.

[3] J. Sieniawski, W. Ziaja, K. Kubiak, and M. Motyka, J. Sieniawski and W. Ziaja, eds. "Microstructure and mechanical properties of high strength two-phase titanium alloys," in *Titanium Alloys - Advances in Properties Control*, London: IntechOpen Limited, 2013, pp. 69-80.

[4] F. Torrent, L. Lavisse, P. Berger, J. M. Jouvard, H. Andrzejewski, G. Pillon, S. Bourgeois, and M. C. Marco de Lucas, "Wavelength influence on nitrogen insertion into titanium by nanosecond pulsed laser irradiation in air," *Applied Surface Science*, vol. 278, pp. 245-249, 2013.

[5] B. Yilbas, S. Akhtar, and O. Keles, "Laser straight cutting of Ti-6Al-4V alloy: Temperature and stress fields," in *Materials and Surface Engineering*, J. P. Davim, ed. Woodhead Publishing Reviews: Mechanical Engineering Series, UK: Woodhead Publishing, 2012, pp. 243-265.

[6] I. A. Almeida, W. de Rossi, M. S. F. Lima, J. R. Berretta, G. E. C. Nogueira, N. U. Wetter, and N. D. Vieira, "Optimization of titanium cutting by factorial analysis of the pulsed Nd:YAG laser parameters," *Journal of Materials Processing Technology*, vol. 179, pp. 105-110, 2006.

[7] J. D. Majumdar, "Laser Gas Alloying of Ti-6Al-4V," *Physics Procedia*, vol. 12, pp. 472-477, 2011.

[8] Y. Yin, L. Hang, S. Zhang, and X. L. Bui, "Thermal oxidation properties of titanium nitride and titanium–aluminum nitride materials - A perspective for high temperature air-stable solar selective absorber applications," *Thin Solid Films*, vol. 515, pp. 2829-2832, 2007.

[9] F. H. Pollard and P. Woodward, "The stability and chemical reactivity of titanium nitride and titanium carbide," *Transactions of the Faraday Society*, vol. 46, pp. 190-199, 1950.

[10] D. P. Satko, J. B. Shaffer, J. S. Tiley, S. L. Semiatin, A. L. Pilchak, S. R. Kalidindi, Y. Kosaka, M. G. Glavicic, and A. A. Salem, "Effect of microstructure on oxygen rich layer evolution and its impact on fatigue life during high-temperature application of α/β titanium," *Acta Materialia*, vol. 107, pp. 377-389, 2016.

[11] T. Zhang, Z. Wu, R. Hu, F. Zhang, H. Kou, and J. Li, "Influence of nitrogen on the microstructure and solidification behavior of high Nb containing TiAl alloys," *Materials & Design*, vol. 103, pp. 100-105, 2016.

[12] L. D. Scintilla, L. Tricarico, A. Wetzig, and E. Beyer, "Investigation on disk and CO2 laser beam fusion cutting differences based on power balance equation," *International Journal of Machine Tools and Manufacture*, vol. 69, pp. 30-37, 2013.

[13] O. O. Kardas, O. Keles, S. Akhtar, and B. S. Yilbas, "Laser cutting of rectangular geometry in 2024 aluminum alloy: Thermal stress analysis," *Optics & Laser Technology*, vol. 64, pp. 247-256, 2014.

[14] O. S. Bursi, M. D'Incau, G. Zanon, S. Raso, and P. Scardi, "Laser and mechanical cutting effects on the cut-edge properties of steel S355N," *Journal of Constructional Steel Research*, vol. 133, pp. 181-191, 2017.

[15] C. H. Fu and Y. B. Guo, "Laser cutting simulation of nitinol stent alloy with moving heat flux," presented at The International Conference on Shape Memory and Superelastic Technologies American Society for Metals, Pacific Grove, CA, May 12-16, 2014.

[16] L. Shanjin and W. Yang, "An investigation of pulsed laser cutting of titanium alloy sheet," *Optics and Lasers in Engineering*, vol. 44, pp. 1067-1077, 2006.

[17] A. Kumar Pandey and A. Kumar Dubey, "Simultaneous optimization of multiple quality characteristics in laser cutting of titanium alloy sheet," Optics & Laser Technology, vol. 44, pp. 1858-1865, 2012.

[18] H. Ozaki, M. Q. Le, H. Kawakami, J. Suzuki, Y. Uemura, Y. Doi, M. Mizutani, and Y. Kawahito, "Real-time observation of laser cutting fronts by X-ray transmission," *Journal of Materials Processing Technology*, vol. 237, pp. 181-187, 2016.

[19] H. G. Salem, M. S. Mansour, Y. Badr, and W. A. Abbas, "CW Nd:YAG laser cutting of ultra low carbon steel thin sheets using O_2 assist gas," *Journal of Materials Processing Technology*, vol. 196, pp. 64-72, 2008.